JACS
JOURNAL OF THE AMERICAN CHEMICAL SOCIETY
pubs.acs.org/JACS
Article

Labile Iron Pool of Isolated *Escherichia coli* Cytosol Likely Includes Fe-ATP and Fe-Citrate but not Fe-Glutathione or Aqueous Fe

Hayley N. Brawley,[§] Alexia C. Kreinbrink,[§] Justin D. Hierholzer, Shaik Waseem Vali, and Paul A. Lindahl*

Cite This: *J. Am. Chem. Soc.* 2023, 145, 2104–2117
Read Online
ACCESS | Metrics & More | Article Recommendations | Supporting Information

ABSTRACT: The existence of labile iron pools (LFePs) in biological systems has been recognized for decades, but their chemical composition remains uncertain. Here, the LFeP in cytosol from *Escherichia coli* was investigated. Mössbauer spectra of whole vs lysed cells indicated significant degradation of iron-sulfur clusters (ISCs), even using an unusually gentle lysis procedure; this demonstrated the fragility of ISCs. Moreover, the released iron contributed to the non-heme high-spin Fe(II) species in the cell, which likely included the LFeP. Cytosol batches isolated from cells grown with different levels of iron supplementation were passed through a 3 kDa cutoff membrane, and resulting flow-through-solutions (FTSs) were subjected to SEC-ICP-MS. Mössbauer spectroscopy was used to evaluate the oxidation states of standards. FTSs exhibited iron-detected peaks likely due to different forms of Fe-citrate and Fe-nucleotide triphosphate complexes. Fe-Glutathione (GSH) complexes were not detected using physiological concentrations of GSH mixed with either Fe(II) or Fe(III); Fe(II)-GSH was concluded not to be a significant component of the LFeP in *E. coli* under physiological conditions. Aqueous iron was also not present in significant concentrations in isolated cytosol and is unlikely a major component of the pool. Fe appeared to bind ATP more tightly than citrate, but ATP also hydrolyzed on the timescale of tens of hours. Isolated cytosol contained excess ligands that coordinated the added Fe(II) and Fe(III). The LFeP in healthy metabolically active cells is undoubtedly dominated by the Fe(II) state, but the LFeP is redox-active such that a fraction might be present as stable and soluble Fe(III) complexes especially under oxidatively stressed cellular conditions.

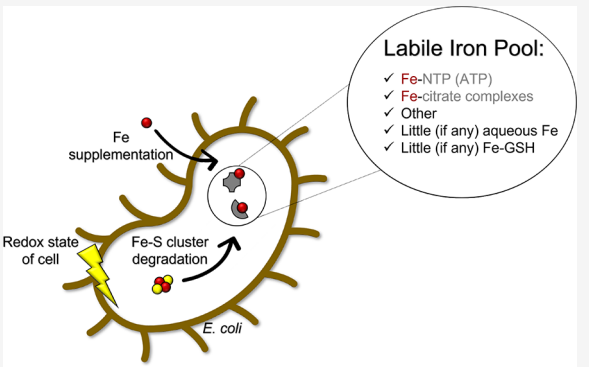

INTRODUCTION

Iron plays essential roles in biology due to its remarkable electronic, substrate-binding, and catalytic properties.[1−4] However, installing this redox-active d-block transition metal into client proteins and enzymes requires that nutrient iron enters the cell and traffics through it. Iron trafficking remains poorly characterized despite a half-century of investigations, due in large part to the inherent lability of iron trafficking complexes. However, lability is essential, for these complexes must be sufficiently labile to deposit their cargo into client apo-proteins but not so labile as to release it into cytosol as aqueous iron.[5] Aqueous iron and many labile Fe(II) complexes promote deleterious side reactions with O_2 and derivatives such as H_2O_2.[6] Reactive oxygen species generated by these side reactions can damage nucleic acids, proteins, and other essential cellular macromolecules. How the cell balances these opposing requirements might be revealed if the chemical composition of the labile iron pool (LFeP) were better understood.

The LFeP is thought to consist of low-molecular-mass (LMM) Werner-type complexes in which iron is coordinated by non-proteinaceous ligands with O, N, and/or S donors. Starting in the 1970s, extracts from mainly mammalian cells were subjected to size-exclusion (SEC) and/or ion-exchange chromatography and various LMM iron species were isolated and identified as candidates for the pool. In 1972, Konopka and Szotor used ion-exchange chromatography to detect the LFeP in the acid-soluble fraction of erythrocyte extracts.[7] They concluded that the LFeP consisted of iron bound to ATP, ADP, AMP, and NADP. Indeed, Fe(III)-ATP complexes are quite stable.[8] A few years later, Bartlett isolated an Fe(III)-GTP complex from extracts of rat and human erythrocytes.[9] Other trafficking complexes were also reported, including Fe-citrate as a constituent of the LFeP in rat reticulocyte cytosol.[10] Weaver and Pollack added ^{59}Fe to lysed isolated reticulo-

Received: June 23, 2022
Published: January 20, 2023

ACS Publications
© 2023 The Authors. Published by American Chemical Society

https://doi.org/10.1021/jacs.2c06625
J. Am. Chem. Soc. 2023, 145, 2104–2117

cytes.[11] They filtered the resulting solution to remove proteinaceous species and applied the flow-through-solution (FTS) to an ion-exchange column. The major species detected was ^{59}Fe-ATP, which they concluded was the major component of the LFeP. Fe-AMP was also detected, but Fe-GTP was not.

By the early 1990s, the preferred approach to detecting and quantifying the LFeP had shifted to custom-designed fluorescence-based membrane-permeable chelator probes.[12−15] This occurred perhaps out of concern that species isolated chromatographically might be artifacts generated during cell lysis and subsequent manipulations. In contrast, chelator probes could penetrate intact, metabolically active cells.[12−14] Once inside, they could bind iron from the endogenous LFeP, altering their fluorescent properties and thereby allowing detection and quantification.

A second concern with characterizing LFePs isolated from cell extracts was that the iron might oxidize. Rothman et al. treated cultured rat hepatocytes with deferoxamine and detected a pool of ferric ions that could be used for heme synthesis and stored as ferritin.[16] However, prior to this, Egyed and Saltman reported that iron in metabolically active, aerobically grown cells was ferrous.[17] Most subsequent studies support the dominance of Fe(II) in the LFeP though the presence of Fe(III) complexes within this pool has been suggested.[18−21]

By using the chelator calcein to detect the LFeP in human K562 cells, Cabantchik and coworkers concluded that the iron in these pools was Fe(II), and they quantified the size of the LFeP to be ∼0.5 μM.[18] However, pool size is sensitive to the concentration (and type) of iron included in the growth medium.[22] The estimated concentration of LFeP in erythroid and myeloid cells ranges from 0.2-1.5 μM.[23] Petrat, Rauen, and deGroot used chelators to detect the LFeP in rat hepatocytes and concluded that the pool was larger, namely, 4-10 μM.[24−26] This variability might arise because chelator-based methods define the LFeP operationally—as that obtained by adding a particular chelator at a defined concentration, duration, and temperature.[19] Thus, different chelators and conditions might afford different pool-size estimates.

The LFeP in bacteria, especially that in *Escherichia coli*, has also been investigated, albeit with greater emphasis on the magnitude of the pool and its regulation than on chemical composition. The LFeP concentration in healthy *E. coli* has been reported to be ∼10 μM and mostly in the Fe(II) state.[27] The LFeP concentration in *Bacillus subtilis* has a similar range.[28] Using the EPR method developed by Imlay, Kiley and coworkers found that the LFeP in *E. coli* increases from ∼26 μM in aerobic cells to ∼177 μM in anaerobic cells.[29] Using Mössbauer (MB) spectroscopy, Wofford et al. estimated the size of the LFeP in whole *E. coli* cells to be 50-500 μM, depending on the degree to which cultures were exposed to O_2 and the [Fe] in the growth medium.[30] MB spectra of whole *E. coli* cells and FTSs of anaerobically isolated lysates are dominated by a quadrupole doublet with parameters typical of high-spin Fe(II). In *E. coli* and many other bacteria, iron homeostasis is regulated by Fur (Ferric uptake regulator).[31] Historically, Fur was thought to sense and bind mononuclear Fe(II) to repress the Fe import system, but a recent report suggests that it reversibly and sensitively binds a [Fe_2S_2] cluster in accordance with the LFeP concentration.[31]

Hider and coworkers employed a computational approach to characterize the LFeP.[32−34] Using thermodynamic binding affinities of various Fe(II)-ligand complexes along with reported concentrations of candidate ligands in the cytosol and the known redox chemistry of iron, they simulated pH-dependent binding plots to define and quantify the composition of the LFeP. They measured the Fe(II)-GSH binding affinity to be logK_a = 5.4.[32] Although this is not unusually large, the concentration of GSH in the cytosol of cells is unusually high (2−10 mM) relative to many other candidate ligands, and its redox activity (2GSH ⇄ GSSG +2H^+ + 2e^-) maintains labile iron in the reduced state. Based on these considerations, they proposed that Fe(II)-GSH dominates the LFeP in cells, and this proposal is now nearly universally accepted.

In the past decade, we have revisited the chromatography-based approach for investigating LFePs using a bioinert system (no contact of solutions with bio-relevant metal surfaces) located in a refrigerated, inert atmosphere glove box and interfaced to an ICP-MS for sensitive metal-ion detection. Metal-binding ligands and buffers are excluded from cytosol isolation procedures, and our columns are treated in a manner (called zinc-loading) that minimizes the adsorption of metals.[35] With these improvements, we recently characterized labile metal pools in *Saccharomyces cerevisiae* cytosol[36] and the labile nickel pool of *E. coli*.[37] Here, we revisit the LFeP in *E. coli* and report new insights that advance our understanding of these pools.

EXPERIMENTAL SECTION

Cell Growth. Twenty-six batches of MG1655-pZa31mycR cells were cultured aerobically in 50 mL of M9 media containing 0.4% (w/v) glucose and 1 mM chloramphenicol (Sigma-Aldrich) overnight at 37 °C with 200 rpm shaking.[35] These cells contain a plasmid (pZa31mycR) that encodes a endolysin gene, which when expressed, causes cell lysis.[33,38,39] Each batch was transferred to 1 L of media and harvested at mid-exponential phase (OD_{600}∼ 1). The medium for some batches was supplemented with either 10 μM natural-abundance Fe(III)-citrate (Fisher Chemical) or 10 μM ^{57}Fe(III)-citrate (Cambridge Isotopes Laboratories, 95.5% Fe_2O_3). Other batches were supplemented with 100 μM natural-abundance Fe(III)-citrate. Some batches were harvested in a refrigerated anaerobic glove box (Mbraun, Labmaster 130, <5 ppm O_2; <10 °C) and processed under strict anaerobic conditions. Other batches were harvested and processed aerobically and then brought into the box for experiments.

Isolation of Anaerobic Cytosol and FTS. High-purity water (HPW) was house-distilled, passed through deionizing cartridges (Barnstead), and then redistilled using a Teflon sub-boiling still (Savillex). Harvested cells were washed with degassed HPW in an anaerobic glovebox and re-centrifuged (Sorvall Lynx 6000 Centrifuge) at 4000*g* for 10 min. Cells were resuspended anaerobically in degassed 20 mM ammonium bicarbonate (ABC) pH 7.2 buffer in a 15 mL plastic (Falcon) tube (1 mL/g of cells, ∼5 g cells per culture), and the tube was placed in a 1 L centrifuge bottle. The bottle was sealed, frozen in liquid N_2, and stored at −80 °C. Frozen cells in the sealed bottle were thawed at 37 °C with 100 rpm shaking for 1 h and returned to the glovebox. The Falcon tube containing lysate was wrapped with electrical tape and centrifuged at 10,000*g* for 5 min. The supernatant was transferred to a fresh Falcon tube and incubated with 1.12 mg/mL DNase (Sigma-Aldrich) and 10 mM $MgCl_2$ (4 μL/g of cell pellet). The tube was resealed in the 1 L centrifuge bottle and incubated for 30 min at 37 °C with 100 rpm shaking. The lysate was transferred anaerobically to centrifuge tubes and spun at 100,000*g* for 60 min (SW32 Ti rotor; Beckman Coulter Optima L-90 K). The resulting supernatant was then passed through either an Ultracel regenerated cellulose 3 kDa ultrafiltration disc (EMD Millipore) or an Ultracel Amicon Ultra 2 mL regenerated cellulose 3 kDa centricon filter (EMD Millipore). The filtered solution was defined as FTS.

https://doi.org/10.1021/jacs.2c06625
J. Am. Chem. Soc. 2023, 145, 2104−2117

Iron Salts and Standards. A solution-mimicking cytosol, called pseudo-flow-throuogh solution (pFTS), was prepared in either 20 mM ammonium acetate (AA) (Sigma-Aldrich) pH 6.5, or in 20 mM ABC (Sigma-Aldrich) pH 7.5. These solutions contained (final concentrations) 2 mM sodium citrate (Fisher Chemical), 5 mM reduced glutathione (GSH) (Sigma-Aldrich), 500 μM disodium oxidized glutathione (GSSG) (Sigma-Aldrich), 5 mM disodium ATP (Sigma-Aldrich), 500 μM sodium ADP (Sigma-Aldrich), 200 μM disodium AMP (Sigma-Aldrich), 100 μM L-cysteine (Sigma-Aldrich), 50 mM sodium glutamate (Sigma-Aldrich), 5 mM L-aspartate (MP Biomedicals), 70 μM L-histidine (MP Biomedicals), 5 mM disodium phosphate (Sigma-Aldrich), and 3 kDa filtered sodium polyphosphate (Sigma-Aldrich) as described.[37] To this was added 2 μM iron from a stock of acidic 1 mM ^{57}Fe(III) prepared as described below. A 50 mM stock of natural-abundance $FeSO_4$ was additionally prepared by dissolving ferrous sulfate hexahydrate (Fisher Chemical) in HPW.

A 1 mM acidic ^{57}Fe(III) stock was prepared by dissolving 40.5 mg of $^{57}Fe_2O_3$ in 2.0 mL of concentrated H_2SO_4 (Sigma-Aldrich). The mixture was covered, heated, and stirred overnight. Once dissolved, the solution was cooled, and 248 mL of HPW was added incrementally. A 50 mM stock of acidic ^{57}Fe(III) was similarly prepared using 405 mg $^{57}Fe_2O_3$ and 10 mL of concentrated H_2SO_4. Both solutions were filtered through a 0.22 μm Stericup filter (Corning), degassed on a Schlenk line, and then stored anaerobically in an N_2-atmosphere glove box at 5−10 °C. A 317 mM acidic ^{57}Fe(III) stock was prepared similarly by dissolving 80 mg of ^{57}Fe metal in 3.7 mL of concentrated trace-metal-grade (TMG) HNO_3 (Fisher Chemical) and 1.0 mL of HPW in a 15 mL polypropylene centrifuge tube (Corning).

For chromatography, individual standard iron complexes were prepared by mixing either aqueous Fe(II) or acidic ^{57}Fe(III) with stock solutions of individual ligands as previously described[35] to a final concentration of 2 μM Fe and the desired concentration of ligand. Standards were prepared on the day before analysis and maintained anaerobically at 5−10 °C prior to use.

Mössbauer Spectroscopy. For Mössbauer (MB) spectroscopy, stock solutions of 500, 50, and 10 mM ATP and citrate, 250 and 50 mM GSH, and 20 mM ascorbate (Acros Organics) were prepared anaerobically in the glove box using HPW or 100 mM ABC pH 7.5 buffer that had been degassed on a Schlenk line prior to import into the box. MB standards were prepared anaerobically by adding acidic ^{57}Fe(III) to the buffer followed by addition of ligand stock solutions. Degassed 1 M TMG NaOH (END Millipore) or 1 M TMG H_2SO_4 (Sigma) were typically used to adjust the final pH of standards to 7.5. Table S1 includes a list of Mössbauer standards (with final concentrations) and spectral parameters. MB spectra were collected on a MS4 WRC spectrometer (SEE Co, Edina MN) at ∼5 K and 0.05 T. The magnetic field was applied parallel to the gamma radiation. An α-iron foil was used for room temperature calibration.

For whole-cell MB studies, cells were grown in media supplemented with 10 μM ^{57}Fe(III)-citrate. One batch was harvested and processed anaerobically. Cells were washed and pelleted into a MB cup and then frozen in liquid nitrogen. After a MB spectrum was collected, the frozen sample was imported into the glove box, thawed, and incubated in the cup for 30 min at 37 °C. The sample was refrozen, and another spectrum was collected. Another batch was harvested and processed similarly but under aerobic conditions.

Chromatography. SEC-ICP-MS was performed initially on a Superdex Peptide 10/300 GL (Cytiva) SEC column and later on a Superdex 30 Increase 10/300 GL (Cytiva) SEC column after production of the Peptide column was discontinued. Columns were housed in a glovebox at 5−10 °C, connected to an ICP-MS (Agilent 7700x), and zinc-loaded.[35] Four mobile phases were used, including 20 mM AA at pH 5.5 and 6.5, and 20 mM ABC pH 7.5 with/without 50 μM sodium dithionite (Sigma-Aldrich). Each mobile phase was filtered and degassed as described.[35] To assess the proportion of iron in samples that adhered to the columns, some samples were injected onto a "ghost column" composed of PEEK tubing in place of a column.

A 0.5 M NaOH (EMD Chemicals) stock solution in HPW was degassed and stored in the box. A 1.0 M sodium dithionite stock was prepared anaerobically by dissolving ∼1.74 g of sodium dithionite (Sigma-Aldrich) in 0.2 M NaOH (from 0.5 M stock) and stored anaerobically for months. The stock was diluted into the desired mobile phase (1 L or greater total volume) anaerobically, and the final pH of the mobile phase was minimally affected. Sodium dithionite is more stable at pH 7.5 than at 6.5, so it was only included in pH 7.5 buffer. Buffers were thoroughly degassed and imported into the box prior to adding dithionite. This allowed low concentrations of dithionite to be effective in making solutions overall reducing. Salts became increasingly problematic using higher dithionite concentrations, causing the signal/noise of the chromatograms (especially those detecting ^{34}S) to decline. A 10 mM stock of methyl viologen (Sigma-Aldrich) was prepared in HPW. The reducing ability of the mobile phase eluting from the column was qualitatively assessed by a clear-to-blue color change due to reduction of methyl viologen.

Elemental Analysis. A series of five ICP-MS iron calibration standards were prepared with a custom-made TEXASAM-15REV3 stock (Inorganic Ventures). The most concentrated stock standard solution contained 1 mg/L of natural-abundance iron. The remaining standards were obtained by diluting the previous standard 10-fold. The final concentration of TMG HNO_3 in each standard was 0.5% (v/v) except for the stock, which was 5%. Two blanks of 0.5% HNO_3 accompanied this standard set. An internal standard solution, IV-ICPMS-71D (Inorganic Ventures), was also prepared in 0.5% HNO_3.

For elemental analyses, three aliquots (100 μL) of lysate, cytosol, and FTS from three batches of aerobically isolated cells were transferred into 15 mL polypropylene centrifuge tubes (Corning). Five hundred microliters of 5% HNO_3 were added to each tube. Tubes were capped, sealed with electrical tape, vortexed, and incubated at 80 °C for 24−48 h depending on the amount of protein in the sample. Samples were cooled to room temperature and diluted to 5.0 mL with HPW. Resulting solutions were analyzed by ICP-MS in collision mode with 5.0 mL/min H_2 flow. The back-calculation of metal concentrations in samples has been described.[35]

RESULTS

MB Spectra of *E. coli* Cells and Lysate. Our initial aim was to characterize the LFeP in *E. coli* cytosol by combining MB spectroscopy with improved liquid chromatography methods. In general, we isolated cytosol from lysed cells, removed the high-molecular-mass (i.e. protein) fraction, and passed the resulting FTS through an SEC column that resolved LMM iron species. Chromatograms were compared to those of candidate Fe complexes. MB spectroscopy was used to evaluate the oxidation state of selected iron standards.

A major challenge in the field is to prevent or minimize perturbations in either the composition or redox state of the LFeP during cell lysis, cytosol isolation, and subsequent chromatography. To address this, whole *E. coli* cells were harvested anaerobically, similar to earlier reports,[30] and investigated by MB spectroscopy. The whole-cell spectrum (Figure 1A) was dominated by two quadrupole doublets, including one with isomer shift and quadrupole splitting parameters typical of both $[Fe_4S_4]^{2+}$ clusters and low-spin Fe(II) hemes, and the other with parameters typical of non-heme high-spin (NHHS) Fe(II); MB parameters are given in Table S1. The latter doublet reflected all NHHS Fe(II) species in the cell, including those bound to proteins as well as those associated with the LFeP. After collecting the spectrum, cells were lysed under anaerobic conditions, and a spectrum of the cell lysate was obtained (Figure 1B). The spectrum revealed that about 9% of cellular iron had converted into NHHS Fe(II) (see area percentages in Table S1). To be clear, in this experiment a frozen whole-cell sample was thawed in an

https://doi.org/10.1021/jacs.2c06625
J. Am. Chem. Soc. 2023, 145, 2104−2117

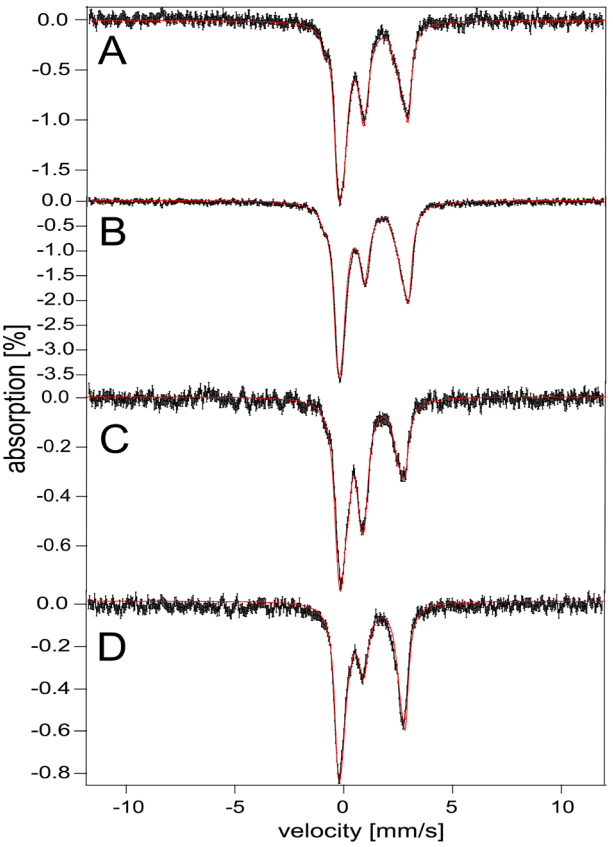

Figure 1. Low-temperature low-field (5 K, 0.05 T) Mössbauer spectra of matched *E. coli* whole cells and lysates. Cells were grown aerobically in minimal media supplemented with 10 μM ^{57}Fe(III)-citrate and harvested at mid-exponential growth (OD_{600} ~ 1). (A) whole cells; (B) lysed cells from (A) thawed anaerobically at 37 °C and incubated 30 min; (C) whole cells from another batch grown equivalently; (D) lysed cells from (C) thawed aerobically at 37 °C and incubated for 30 min. Red lines are simulations using components and parameters in Table S1.

anaerobic environment, incubated 30 min at 37 °C in its MB cup, and then refrozen. Despite this unusually gentle treatment, 17% of cellular ISCs were damaged and the iron from these clusters was released as NHHS Fe(II). These results reveal the remarkable fragility of ISCs bound to proteins in *E. coli*.

Another whole-cell sample was lysed under aerobic conditions. In this case, 20% of the total iron in the cell was released from 40% of cellular ISCs during lysis, and they again contributed to the NHHS Fe(II) pool (Figure 1C,D). This experiment again illustrates the extreme fragility of ISCs in the cell as well as the enhancing effect of O_2.

SEC-ICP-MS Chromatography of FTS. The soluble portion of lysed cells was passed through a 3 kDa cutoff membrane under anaerobic conditions, and the resulting FTS was analyzed by SEC-ICP-MS using a mobile phase of degassed 20 mM AA pH 6.5. The size of the LFeP was affected by the level of iron supplementation in the growth media. The FTS from cells that were supplemented with 10 or 100 μM Fe(III)-citrate exhibited numerous species in the LMM region (Figure 2, B and C), which we attributed collectively to the LFeP. Fitting the peaks required at least 5-6 terms as indicated by the gray Gaussian lines underneath the traces (the composite simulations are in blue; fitting parameters in

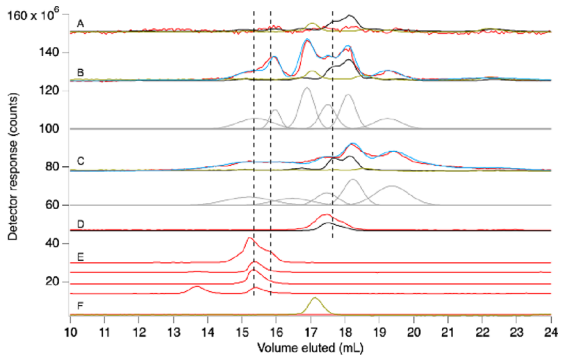

Figure 2. SEC-ICP-MS chromatograms at pH 6.5 of FTS isolated anaerobically from cells grown aerobically in media with different levels of iron supplementation and various Fe standards. (A) FTS from cells grown in media without iron supplementation; (B) same as (A) but from cells supplemented with 10 μM Fe(III) citrate; (C) same as (A) but from cells supplemented with 100 μM Fe(III)-citrate (averaged n = 3). The blue lines in (B) and (C) are overall simulations composed of 6 iron peaks, shown below in gray. Fitting details are given in Table S2. (D-F), standards composed of 2 μM $FeSO_4$ plus (D) 1000 μM ATP; (E) 5000, 1000, 500, and 250 μM citrate, top to bottom; (F) 1000 μM GSH. Dashed vertical lines represent elution volumes of Fe species coeluting with standards. Chromatograms obtained from the Superdex 30 Increase column. Color coding: ^{56}Fe, red; ^{57}Fe, maroon; ^{31}P, black; ^{34}S, yellow; composite simulations, blue; individual simulation terms, gray. Multiplication factors: (A) ^{56}Fe × 3000, ^{31}P × 10, ^{34}S × 600; (B) ^{56}Fe × 1000, ^{31}P × 10, ^{34}S × 600; (C) ^{56}Fe × 1000, ^{31}P × 10, ^{34}S × 600; (D) ^{56}Fe × 100, ^{31}P × 5; (E) ^{56}Fe × 100; (F) ^{56}Fe × 100; ^{34}S × 400.

Table S2). The FTS from unsupplemented cells exhibited fewer peaks and lower intensities (Figure 2A). Correcting for the 4-fold dilution used in isolating cytosol, the iron concentration in undiluted FTS from unsupplemented cells was calculated to be ~2 μM (Table S3). Most of this iron adhered to the column, explaining the low observed peak intensities.

Fe(II)-citrate standards migrated in a similar chromatographic region (Figure 2E). The coordination chemistry of Fe-citrate is complicated,[40] so it was not surprising that its chromatographic properties varied with the ratio of citrate:Fe concentrations. Using 250 μM citrate and 2 μM Fe(II), two peaks were observed at elution volumes of 13.5 and 15.3 mL. With increasing concentrations of citrate, the 13.5 mL peak intensity declined while the 15.5 mL peak intensity increased. Using the highest citrate concentration, additional peaks developed, including one at 15.8 mL. This peak and the one at 15.5 mL approximately comigrated with peaks in FTS from cells supplemented with 10 and 100 μM Fe (Figure 2 B and C).

Another set of experiments was performed using aerobically prepared FTS (called aFTS), and Fe standards were prepared using acidic ^{57}Fe(III) rather than Fe(II). The lysate filtering step and the chromatography experiment were performed in the glove box using degassed mobile phase buffer. Thus, O_2 exposure was modest. Interestingly, the chromatograms were similar overall to those obtained using anaerobically prepared FTS. Thus, we were unable to establish the oxidation state of iron in FTS from LC traces. One possibility is that the Fe complexes that compose the LFeP migrated similarly regardless of iron redox state (we present some evidence for this below). Another possibility, supported by the MB study of

https://doi.org/10.1021/jacs.2c06625
J. Am. Chem. Soc. 2023, 145, 2104−2117

Figure 1, is that the reducing environment of the cell lysate retained the Fe(II) state of the aFTS despite the brief exposure to O_2. Currently, we cannot distinguish these possibilities.

Chromatograms of aFTS using pH 7.5 mobile phase exhibited three major iron-detected peaks with elution volumes of 14.5, 15.8, and 18.2 mL (Figure 3A, red line and vertical

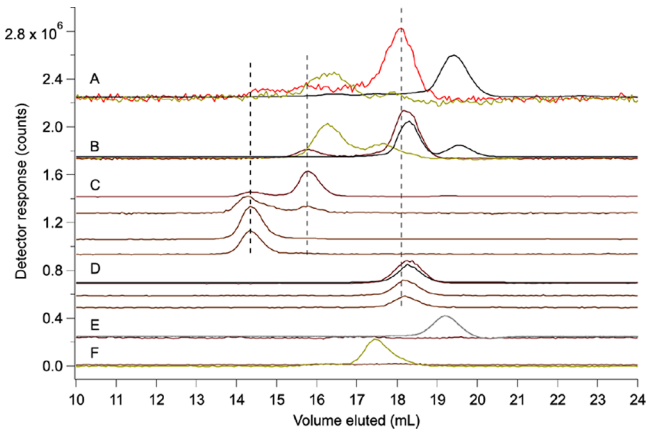

Figure 3. SEC-ICP-MS chromatograms of *E. coli* aFTS at pH 7.5. (A) Averaged aFTS (n = 3); (B) pFTS; (C-F) standards composed of 2 μM dilute acidic ^{57}Fe(III) plus (C) 5000, 1000, 500, and 250 μM citrate, top-to-bottom; (D) 5000, 1000, and 500 μM ATP, top-to-bottom; (E) 1000 μM histidine; (F) 10,000 μM GSH. Dashed vertical lines represent elution volumes of major Fe species. Chromatograms were obtained with a Superdex Peptide column. Color coding is the same as Figure 2 except gray is absorbance at 210 nm. Multiplication factors: (A) ^{56}Fe × 200; ^{31}P × 1; ^{34}S × 200; (B) ^{57}Fe × 6, ^{31}P × 0.25; ^{34}S × 10; (C) ^{57}Fe × 6 for 5000, ^{57}Fe × 30 for 1000, ^{57}Fe × 4 for 500, ^{57}Fe × 15 for 250; (D) ^{57}Fe × 10 for 5000; ^{57}Fe × 10 for 1000 and 500, ^{31}P × 0.1 for 5000; (E) ^{57}Fe × 10, A210 × 2000; (F) ^{57}Fe × 10, ^{34}S × 6.

dashed lines). Peak elution volumes differed from those of Figure 2 because the column was different (Superdex Increase in Figure 2 vs the discontinued Peptide column in Figure 3). pH differences also affected elution volumes. We previously reported similar peaks for LC-ICP-MS traces of cytosolic FTS but with different intensity ratios (see Figure 9 of ref 35). Peak intensity ratios in current batches also varied, and so the average of three batches is displayed. The corresponding S trace (yellow line) included a major peak at 16.5 mL and a minor one at 17.3 mL. The corresponding P trace (black line) included a major peak at 19.2 mL and 2−3 minor peaks between 16−18 mL.

The pFTS was prepared by combining citrate, ATP, ADP, AMP, GSH, GSSG, His, Asp, Glu, Cys, phosphate, and polyphosphate at concentrations similar to those in *E. coli* cytosol[41] and buffered at physiological pH. We then added 2 μM (final concentration) aqueous ^{57}Fe(III) in dilute acid. The resulting pFTS exhibited two dominant Fe peaks (Figure 3B) that comigrated with the aFTS peaks at 15.8 and 18.2 mL. Two S peaks were also evident in aFTS traces (Figure 3B, yellow line); these were assigned to oxidized and reduced glutathione (GSSG and GSH) based on the elution volume of free GSH (Figure 3F) and GSSG (Figure S2ii). Phosphorus traces of pFTS included a major peak at 19.2 mL (as observed in aFTS) and another at 18.2 mL (less intense in aFTS traces). Based on comigration with standards, we assigned the 19.2 mL P peak to phosphate ions. The 18.2 mL peak is assigned below.

Fe-citrate standards were prepared by mixing 2 μM acidic ^{57}Fe(III) with increasing concentrations of citrate (250−5000 μM final concentrations in 20 mM ABC pH 7.5 buffer). A similar ratio-dependent peak pattern was observed as in Figure 2. Resulting solutions exhibited two peaks, which comigrated with two Fe peaks in the aFTS, namely, at 14.5 and 15.8 mL (Figure 3C, four maroon lines). Their intensities varied with the concentration of citrate used; lower concentrations favored the 14.5 mL peak, while higher concentrations favored the 15.8 mL peak. This behavior suggested that these Fe peaks arose from two different Fe-citrate complexes.

We also examined the chromatographic properties of aFTS using a mobile phase of 20 mM AA at pH 6.5 and 5.5. At pH 6.5, aFTS exhibited two major Fe peaks (Figure 4A), which

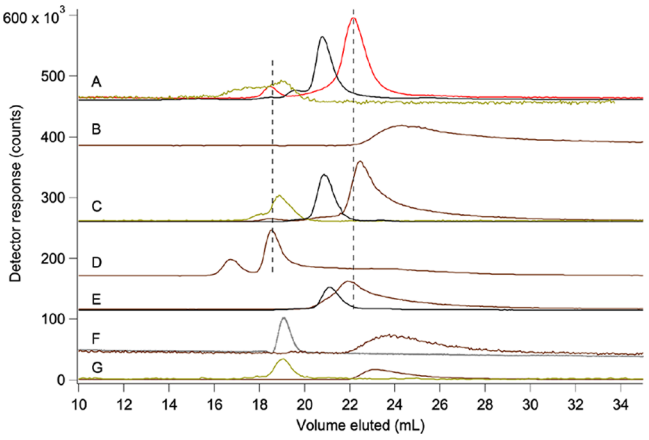

Figure 4. SEC-ICP-MS chromatograms of *E. coli* aFTS and standards at pH 6.5. (A) Averaged aFTS (n = 9); (B) 2 μM dilute acidic ^{57}Fe(III). (C) pFTS; (D−G) 2 μM dilute acidic ^{57}Fe(III) plus 1.0 mM (D) citrate, (E) ATP, (F) His, or (G) GSH. Chromatograms were obtained with a Superdex Peptide column. Color coding is the same as in Figure 3. Multiplication factors: (A) ^{56}Fe × 3, ^{31}P × 0.25, ^{34}S × 30; (B) ^{57}Fe × 2; (C) ^{57}Fe × 1.5; ^{31}P × 0.1, ^{34}S × 2; (D) ^{57}Fe × 0.3; (E) ^{57}Fe × 1, ^{31}P × 0.25; (F) ^{57}Fe × 20, Abs210 × 100; (G) ^{57}Fe × 0.1, ^{34}S × 1.5.

were similar to those obtained using a mobile phase pH of 7.5. Differences in LC traces were likely due to differences in mobile phase pH as well as batch-to-batch variation. The peak at 18.5 mL comigrated with one of the two Fe-citrate peaks (Figure 4D). The presence of the intense Fe peak at 16.8 mL in the citrate standard and its absence in aFTS and pFTS (Figure 4C) is contrasted by the experiments at pH 5.5 (Figure S1), for which the 16.8 mL peak dominated traces of both aFTS and the Fe-citrate standard. The stability of Fe-citrate species appears to be pH-dependent.

MB Spectra of Aqueous Fe(II), ^{57}Fe(III), and ^{57}Fe-Citrate Standards. Although we could not establish the oxidation state of iron in FTS, we were able to do so for standards using MB spectroscopy. Two sources of iron were used to prepare standards, including natural-abundance Fe(II), which contains ∼2% ^{57}Fe, and isotopically-enriched ^{57}Fe(III) in dilute acid. A MB spectrum of a natural-abundance buffered Fe(II) sulfate solution exhibited a quadrupole doublet typical of NHHS Fe(II) species, with parameters δ = 1.40 mm/s, ΔE_Q = 3.47 mm/s, and linewidth Γ = 0.27 mm/s (Figure 5A and Table S1). We used two terms rather than one to simulate this and other Fe(II) doublets as doing so improved fits; the parameters listed throughout the main text are weighted

https://doi.org/10.1021/jacs.2c06625
J. Am. Chem. Soc. 2023, 145, 2104−2117

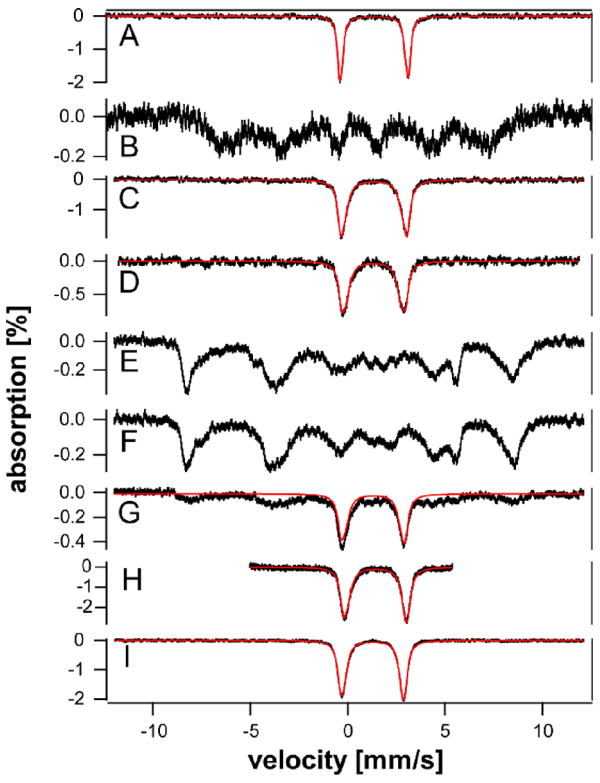

Figure 5. Low-temperature low-field (5 K, 0.05 T) Mössbauer spectra of various iron standards: (A) 50 mM (final concentration) $FeSO_4$ in 100 mM ABC pH 7.5; (B-I) except (G) and (H), 1 mM acidic $^{57}Fe(III)$ in 100 mM ABC pH 7.5, (pH adjusted with TMG NaOH or TMG H_2SO_4 unless denoted) plus (B) nothing, pH unadjusted; (C) 25 mM GSH; (D) 5 mM dithionite; (E) 25 mM citrate; (F) 1000 mM citrate; (G) 500 μM acidic $^{57}Fe(III)$ + 12.5 mM citrate + 200 mM GSH in 100 mM ABC pH 7.5; (H) 500 μM acidic $^{57}Fe(III)$ + 12.5 mM citrate + 200 mM GSH in 100 mM ABC pH 7.5 incubated in anaerobic refrigerated glovebox for 24 h; (I) 25 mM citrate + 5 mM dithionite. Red lines are simulations using parameters in Table S1.

averages. The acidic $^{57}Fe(III)$ stock exhibited a magnetic spectrum indicating the high-spin Fe(III) state (Figure 5B). When the $^{57}Fe(III)$ stock was treated with dithionite, the resulting Fe(II) doublet (Figure 5D) had slightly different average parameters (δ = 1.38 mm/s, ΔE_Q = 3.00 mm/s), and it was broader (Γ = 0.48 mm/s) (Table S1). Similar parameters were obtained upon reduction using ascorbate. This implied that "aqueous Fe(II)" obtained using $FeSO_4$ is not identical to that obtained by treating $^{57}Fe(III)$ with dithionite or ascorbate. We will distinguish these as $Fe(II)_{SO4}$, $^{57}Fe(II)_D$, and $^{57}Fe(II)_A$. We then added 25 mM GSH to an aliquot of the dilute acidic $^{57}Fe(III)$ stock. The resulting MB spectrum (Figure 5C) displayed a quadrupole doublet with parameters that were again similar (but not identical) to $Fe(II)_{SO4}$, $^{57}Fe(II)_D$, and $^{57}Fe(II)_A$ (Table S1). Clearly, GSH reduced $^{57}Fe(III)$, but the resulting doublet was not sufficiently distinct to establish whether an Fe(II)-GSH complex had formed. Using shifts in MB parameters to establish changes in ligand environments was challenging because the observed shifts were modest.

A sample obtained by mixing $^{57}Fe(III)$ with 25 mM citrate exhibited a noticeably different S = 5/2 magnetic spectrum (Figure 5E) relative to that of the $^{57}Fe(III)$ stock. Spectral features shifted slightly when 1000 mM citrate was used (Figure 5F). Both indicate the formation of Fe(III)-citrate complexes with perhaps a different complex obtained depending on citrate concentration, consistent with the rich coordination chemistry of iron-citrate complexes.[40]

We considered whether GSH could reduce Fe(III)-citrate complex(es). The spectrum obtained by treating Fe(III)-citrate with 200 mM GSH (Figure 5G) exhibited two species; 60% was a magnetic species reflecting high-spin Fe(III), and 40% was a quadrupole doublet reflecting high-spin Fe(II). The reducing power of GSH at pH 7.5 ($E^{0\prime}\sim -264$ mV vs NHE) is sufficient to fully reduce aqueous Fe(III) to Fe(II), whereas it only partially reduced the Fe(III)-citrate complex(es), even at a high GSH concentration. Citrate coordination causes the reduction potential(s) of the Fe(III)/Fe(II) couple to decline to $\sim$ 0 mV,[40] but GSH should still be sufficiently powerful thermodynamically to ensure full reduction. This suggested that reduction might be slow (at 4 °C), and so we re-prepared the sample but allowed 24 h of incubation. The resulting spectrum exhibited complete reduction (Figure 5H).

We treated the same Fe(III)-citrate complex(es) with 5 mM of the more powerful reductant sodium dithionite ($E^0\sim -660$ mV vs NHE).[42] The resulting spectrum (Figure 5I) exhibited an Fe(II) quadrupole doublet with parameters δ = 1.32 mm/s and ΔE_Q = 3.13 mm/s (Table S1). These parameters were slightly more distinct from those of the aqueous $Fe(II)_D$ or $Fe(II)_A$ doublet, consistent with the formation of an Fe(II)-citrate complex. They were also somewhat different from those of Figure 5H in which GSH was the reductant.

LFeP Likely Includes Contributions from Fe-ATP and Other Nucleotide Triphosphates. Another significant peak in chromatograms of FTSs approximately comigrated with an Fe(II)-ATP standard at 17.5 mL (Figure 2, B–D). Corresponding P traces (black lines) of Fe(II)-ATP also comigrated, so we tentatively assigned it to Fe-ATP. This assignment was reinforced by chromatograms of aFTS at pH 7.5. In this case, the dominant Fe-detected peak in both aFTS and pFTS chromatograms migrated at 18.2 mL (Figure 3A, red line, and 3B, maroon line), which was similar to the Fe-ATP standard (Figure 3D). In contrast to the situation with Fe-citrate, elution volumes did not shift as the concentration of ATP increased from 500 to 5000 μM. The P peak due to the triphosphate group of ATP was also evident in the pFTS and the Fe-ATP standard. The absence of a distinct P peak associated with Fe-ATP in aFTS (Figure 3A) is explained by the difference in ICP-MS sensitivities; Fe is more sensitive than P. Most P intensity in aFTS was due to free phosphate and various LMM forms including Fe-ATP (some of the P intensity at 18.2 mL arises from ATP). A similar situation may have occurred with aFTS at pH 6.5. In those traces, the dominant Fe peak in the aFTS trace (Figure 4A) approximately comigrated with pFTS (Figure 4C) and with the Fe-ATP standard (Figure 4E). In this case, the major P peaks eluted at a slightly earlier elution volume (21 mL), a portion of which probably arose from ATP.

Iron forms complexes with many other nucleotide triphosphates,[8] so we also examined their chromatographic properties. In separate experiments, CTP, GTP, TTP, and UTP were mixed with Fe(II) and $^{57}Fe(III)$ and then chromatographed. Regardless of oxidation state, all formed stable complexes (Figure 6). Fe-GTP migrated similarly to Fe-ATP (traces iii and i, respectively) as did Fe-CTP, Fe-TTP, and Fe-UTP (traces ii, iv, and v). Thus, Fe-pyrimidine-type NTPs migrated as a group and at lower elution volumes than Fe coordinated to purine-type NTPs. We also mixed Fe(II)

https://doi.org/10.1021/jacs.2c06625
J. Am. Chem. Soc. 2023, 145, 2104–2117

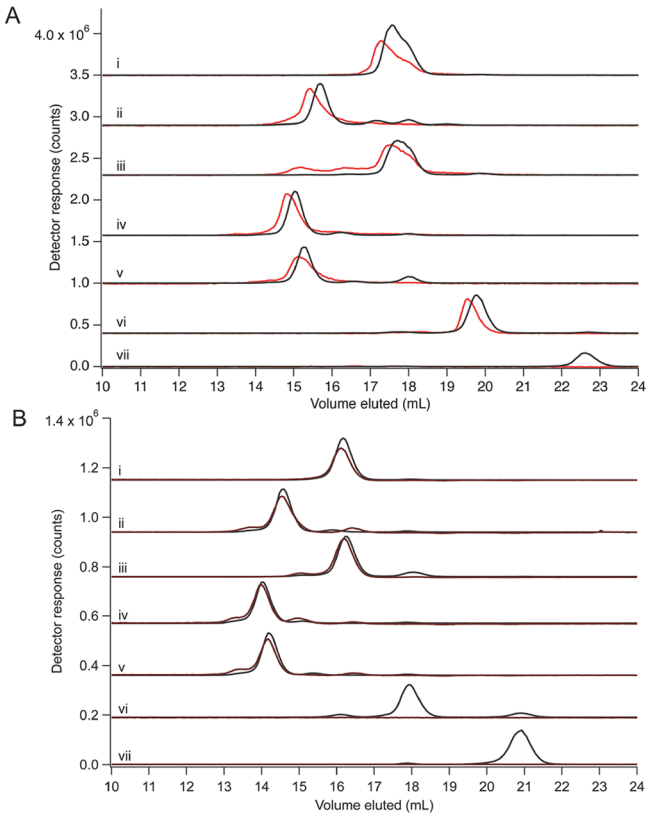

Figure 6. SEC-ICP-MS chromatograms of Fe(II) nucleotide standards at pH 6.5 (Panel A) and Fe(III) nucleotide standards at pH 7.5 (Panel B). Panel A: 2 μM $FeSO_4$ plus 1 mM (final concentration) (i) ATP, (ii) CTP, (iii) GTP, (iv) TTP, (v) UTP, (vi) ADP, or (vii) AMP. Panel B: Same as Panel A but prepared using 2 μM dilute acidic ^{57}Fe(III). Samples in Panel A were run using an AA pH 6.5 mobile phase, whereas samples in Panel B were run using ABC pH 7.5 mobile phase buffer. Multiplication factors: (Panel A) ^{56}Fe × 10, ^{31}P × 1; (Panel B) ^{57}Fe × 5, ^{31}P × 1.25 for (iii), (vi), and (vii).

and ^{57}Fe(III) separately with ADP and AMP. Resulting chromatograms (Figure 6, traces Avii and Bvii) indicated that an Fe-AMP complex did not form. There was some variability as to whether an Fe-ADP complex formed (Figure 6, traces Avi and Bvi). An earlier report found that Fe(III)-ADP binds weakly.[8] We conclude that Fe binds to the triphosphate group of various nucleotides and that these complexes are likely contributors to the LFeP in *E. coli*. We focused on ATP in this study, but the concentrations of many such nucleotides in *E. coli* are in the mM range,[41] and thus, the entire group should be considered as possible if not likely components of the LFeP.

We used MB spectroscopy to investigate the redox and binding properties of ATP. An ^{57}Fe(III)-ATP standard exhibited a magnetic MB spectrum (Figure 7A), indicating high-spin Fe(III). The parameters used in simulating this spectrum were similar to those used to simulate high-spin Fe(III) ions coordinated to polyphosphate chains in isolated vacuoles.[43] This suggested that Fe(III) coordinates the triphosphate group of nucleotide triphosphates.

We attempted to reduce the Fe(III)-ATP sample by adding 200 mM GSH. The resulting spectrum (Figure 7B) displayed partial reduction, similar to the situation with Fe(III)-citrate. Complete reduction was obtained when a sample was incubated for 24 h (Figure 7C). Adding dithionite to a 25

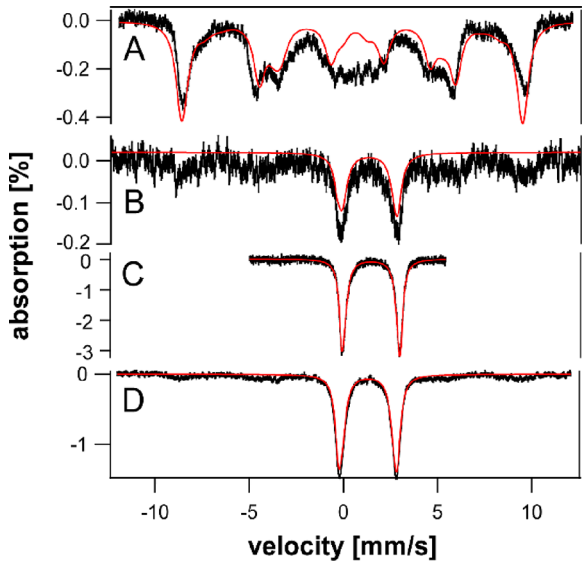

Figure 7. Low-temperature low-field (5 K, 0.05 T) Mössbauer spectra of Fe-ATP standards in 100 mM ABC pH 7.5 buffer. (A) 1 mM acidic ^{57}Fe(III) + 25 mM ATP; (B) 0.5 mM acidic ^{57}Fe(III) + 12.5 mM ATP + 200 mM GSH; (C) 0.5 mM acidic ^{57}Fe(III) + 12.5 mM ATP + 200 mM GSH incubated for 24 h in a refrigerated glovebox; (D) 1 mM ^{57}Fe(III) + 25 mM ATP + 5 mM dithionite. Red lines are simulations using parameters in Table S1.

mM ATP sample also resulted in the Fe(II) state (Figure 7D). The MB parameters used to simulate these quadrupole doublets were shifted slightly relative to aqueous $Fe(II)_D$.

ATP Hydrolysis in the LFeP. The intensity of peaks assigned to Fe-NTP in FTSs varied from batch to batch, and this prompted us to consider whether this behavior arose from ATP hydrolysis occurring in FTS. aFTS was repeatedly freeze-thawed and/or incubated in the glovebox (at 5−10 °C) for different durations to determine whether these procedures affected the LMM Fe species. The chromatogram of ^{56}Fe aFTS that had been frozen immediately after isolation and thawed a few days later exhibited an intense Fe-NTP peak and minor Fe-citrate peaks when run using mobile phase buffer at pH 7.5 that included 50 μM dithionite (Figure 8A). As was evident from the MB studies of Figure 7, dithionite should have reduced the iron to the Fe(II) state for both aFTS and standards. After storing aFTS anaerobically in the box for 72 h, the peak assigned as Fe-NTP declined and the peak attributed to citrate increased (Figure 8B). After storage for 144 h, the Fe-NTP peak at 18 mL was gone, and the Fe-citrate peak at 15.8 mL dominated (Figure 8C). ATP was then added to the aFTS, and the sample was incubated for 1 h and then injected onto the column. The resulting chromatogram was once again dominated by Fe-NTP (Figure 8D). From those experiments, we concluded that (a) Fe-NTP (∼Fe-ATP) was a major LMM Fe species in fresh cytosol aFTS at pH 7.5, (b) ATP in aFTS hydrolyzed over the course of ∼100 h, (c) Fe was released because of hydrolysis, and (d) much of the released Fe coordinated to citrate.

Interestingly, the elution volume in traces of Fe-ATP was unchanged when dithionite was included in the mobile phase (Figure 8G vs Figure 3D). This suggested that Fe(II)-ATP and Fe(III)-ATP had similar chromatographic properties. An Fe(III)-citrate sample analyzed using a mobile phase containing dithionite exhibited a single Fe peak (Figure 8F) that comigrated with one of the Fe-citrate peaks in the aFTS

https://doi.org/10.1021/jacs.2c06625
J. Am. Chem. Soc. 2023, 145, 2104−2117

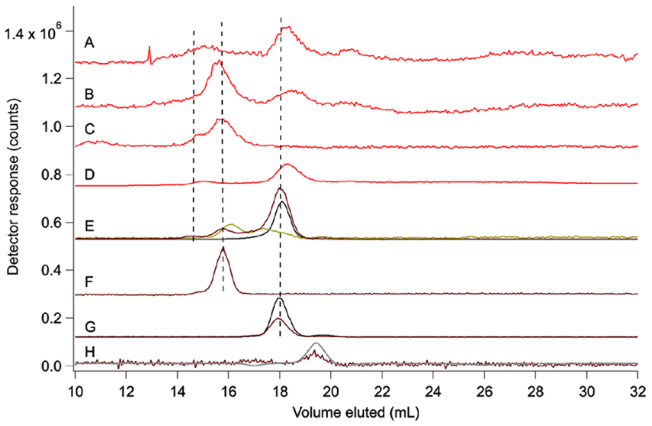

Figure 8. SEC-ICP-MS chromatograms showing ATP hydrolysis in aFTSs under reducing conditions. (A) aFTS (n = 1); (B) same as (A) but after 72 h of incubation in the glovebox at 5−10 °C; (C) same as (A) but after 144 h of incubation in the box; (D) same as (C) but after adding 1 mM ATP; (E) pFTS; (F-H) 2 μM acidic ^{57}Fe(III) + 1 mM (F) citrate; (G) ATP; (H) His. Chromatograms were obtained on a Superdex Peptide column with a mobile phase of 20 mM ABC pH 7.5 + 50 μM dithionite. Color coding as in Figure 3. Magnification factors: (A) ^{56}Fe × 30; (B) ^{56}Fe × 30; (C) ^{56}Fe × 30; (D) ^{56}Fe × 10; (E) ^{57}Fe × 20, ^{31}P × 0.2, ^{34}S × 6; (F) ^{57}Fe × 6; (G) ^{57}Fe × 2, ^{31}P × 0.1; (H) ^{57}Fe × 40, A210 × 1000.

(Figure 8, A−C) and pFTS (Figure 8E). In the absence of dithionite, the same Fe(III)-citrate standard exhibited peaks that comigrated with both Fe-citrate peaks (Figure 3C). This suggested that Fe(II)-citrate AND the form of Fe(III)-citrate obtained using high concentrations of citrate comigrated. This coincidence prevented us from assigning the oxidation state of Fe-citrate complex(es) in aFTS, but it illustrates that the chromatography properties of at least one Fe-citrate complex are not significantly affected by the redox state of Fe in that complex.

Aqueous Iron. Another issue was whether aqueous iron, i.e., Fe, coordinated only by waters and/or hydroxide groups, was a significant component of the LFeP. Using a mobile phase pH of 7.5, dilute acidic ^{57}Fe(III) and Fe(II) adsorbed entirely on the column, and thus, this pH was not useful in assessing this issue (Figure S2Ai,Bi). Using the Peptide column and a mobile phase pH of 6.5 (Figure 4B) or 5.5 (Figure S1B), aqueous Fe(III) exhibited a broad peak at ~25 and ~ 20 mL, respectively. Similar samples run under similar conditions adsorbed onto the Increase column (e.g. Figure S3Bi). We could not explain these differences, so we relied on results obtained with the Peptide column.

Using the Peptide column and at pH 6.5, traces of aFTS did not exhibit a major peak in the aqueous iron region (Figure 4A). At pH 5.5, the resolution between the major Fe peaks of the aFTS and aqueous iron was diminished, but none of the major Fe peaks of the aFTS at pH 5.5 had shapes or elution volumes typical of aqueous Fe (Figure S1). Both results suggested that the LFeP that we isolated does not contain aqueous iron at a significant concentration (less than ca. 10%). The following experiment explains why this might be the case.

Spiking FTS with Iron and Potential Ligands. We suspected that the lack of aqueous iron in FTS was due to the abundance of ligands in the FTS able to bind added Fe(II) or Fe(III). To evaluate this, we isolated FTS and aFTS from cells grown on natural-abundance media unsupplemented with Fe. In separate experiments, we then added increasing amounts of Fe(II) or ^{57}Fe(III) and incubated samples for ≥1 h at 5−10 °C. Untreated FTSs exhibited a few low-intensity peaks (Figure 9, Ai and Bi). With increasing concentrations of either

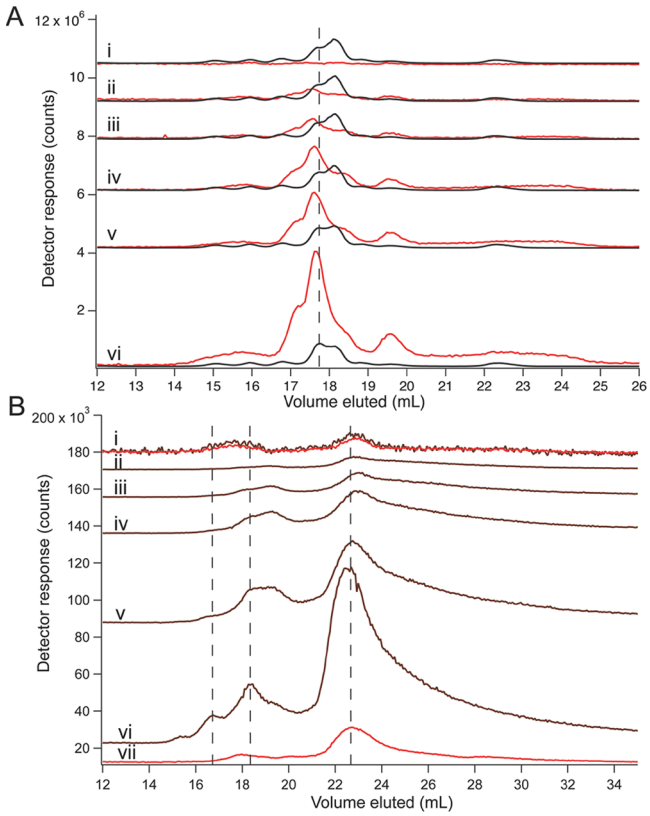

Figure 9. Effect of spiking FTS (Panel A) and aFTS (Panel B) with Fe(II) (A) and Fe(III) at pH 6.5. Panel A: (i) FTS from unsupplemented cells; (ii−vi) same as (i) but with the following (final μM) concentrations of $FeSO_4$ added: (ii) 1; (iii) 2; (iv) 5; (v) 10; (vi) 20. Panel B: same as A but using dilute acidic ^{57}Fe(III); (vii) aFTS from cells supplemented with 100 μM Fe(III) citrate (average of n = 3). Chromatograms in Panel A were obtained with a Superdex Increase column; chromatograms in Panel B were obtained with a Superdex Peptide column. Color coding as in Figure 3. Magnification factors: (Panel A) ^{56}Fe × 50, ^{31}P × 1; (Panel B) (i) ^{57}Fe × 20, ^{56}Fe × 1; (ii−vi) ^{57}Fe × 1; (vii) ^{56}Fe × 1.

Fe(II) or ^{57}Fe(III), the intensities of these peaks increased as did their resolution (Figure 9, Aii−vi and Bii−vi). Additional peaks also appeared. Different columns were used in the two experiments, so only qualitative comparisons were possible. Surprisingly, similar patterns were observed regardless of the oxidation state of iron added. Chromatograms could be divided into three regions, including (from left to right) the citrate region, the NTP region, and a weak-binding region. Overall, approximately 5−6 species contributed. The resolution of the citrate region was greater in panel (B) than in panel (A), but the resolution of the weak-binding region was greater in panel (A) than in panel (B). Peak intensities continued to increase up to and including the samples in which 15 μM iron was added. A similar peak pattern was observed for FTS and aFTS traces from cells supplemented with 100 μM Fe(III)-citrate (Figure 2C and Figure 9Bvii). Correcting for the 4-fold dilution used in isolating cytosol, we estimate that the iron binding capacity of the cytosol from aerobically-grown *E. coli* cytosol is >60 μM. The exact binding capacity

https://doi.org/10.1021/jacs.2c06625
J. Am. Chem. Soc. 2023, 145, 2104−2117

undoubtedly depends on metabolic mode and growth conditions.

We also performed the reverse experiment by adding candidate iron-binding ligands to aFTS. In this particular experiment, only an Fe-citrate peak was initially present (Figure 10A), perhaps due to extensive ATP hydrolysis in that

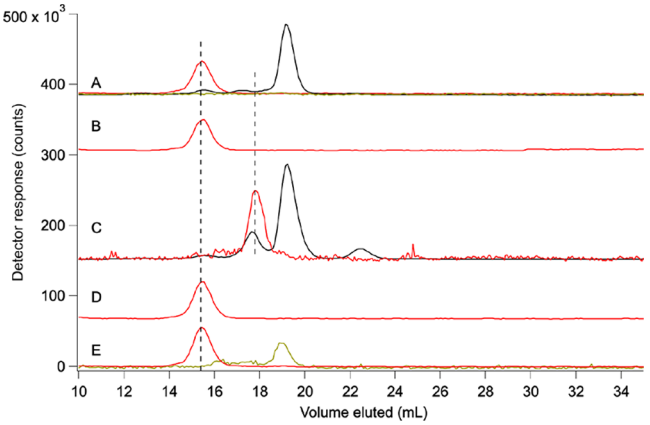

Figure 10. Effect of spiking aFTS at pH 7.5 with candidate ligands to the LFeP. (A) aFTS (n = 1, from unsupplemented cells; (B–E) same as (A) + 1 mM... (B) citrate; (C) ATP; (D) His; (E) GSH. Chromatograms were obtained with a Superdex Peptide column. Color coding as in Figure 3. Magnification factors: (A) ^{56}Fe × 1, ^{31}P × 0.5, ^{34}S × 3; (B) ^{56}Fe × 1; (C) ^{56}Fe × 10, ^{31}P × 0.25; (D) ^{56}Fe × 1; (E) ^{56}Fe × 1, ^{34}S × 5.

sample. Adding citrate, histidine, or GSH to this solution had no effect on the peak (Figure 10, B, D and E), whereas adding ATP caused the abolition of the citrate peak and development of an Fe-NTP peak (Figure 10C). This suggests that Fe-NTP complexes are more stable than Fe-citrate complexes under the conditions examined.

Absence of Fe-GSH in FTS. The most surprising result of this investigation was the absence of an Fe peak in chromatograms of Fe-GSH standards under the conditions investigated. The absence of Fe peaks due to an Fe-GSH complex is evident in Figure 2F (pH 6.5, 2 μM Fe(II) and 1 mM GSH), Figure 3F (pH 7.5, 2 μM Fe(III) and 0.5–10 mM GSH), Figure 4G (pH 6.5, 2 μM Fe(III) and 1 mM GSH), and Figure S1G (pH 5.5, 2 μM Fe(III) and 1 mM GSH). The yellow peaks in these traces are S-detected and indicate free GSH. In Figure 4G, aqueous Fe(II) appears as a broad peak eluting beyond the volume of the GSH peak, again suggesting the absence of an Fe-GSH interaction. Similarly, the broad Fe peak in the trace of Figure S1G suggested aqueous iron or iron that interacted very weakly with GSH.

To further evaluate these unexpected results, we prepared Zn(II)-GSH and Cu(II)-GSH standards as positive controls[44,45] while also attempting to prepare an Fe(II)-GSH complex. Increasing concentrations of GSH, as high as 20 mM, were used. Intense sharp Zn(II)-GSH peaks (Figure 11B, i–vi) and Cu(II)-GSH peaks (Figure 11C, i–vi) were observed, indicating formation of more than one type of stable Zn(II)-GSH and Cu(II)-GSH complexes. Once again no peaks were observed for Fe(II)-GSH (Figure 11A, i–vi).

In another experiment, we included 1 mM GSH in the mobile phase (Figure 11Avi). This was done out of concern that the complex might have formed but then dissociated as it migrated down the column under non-equilibrium conditions.

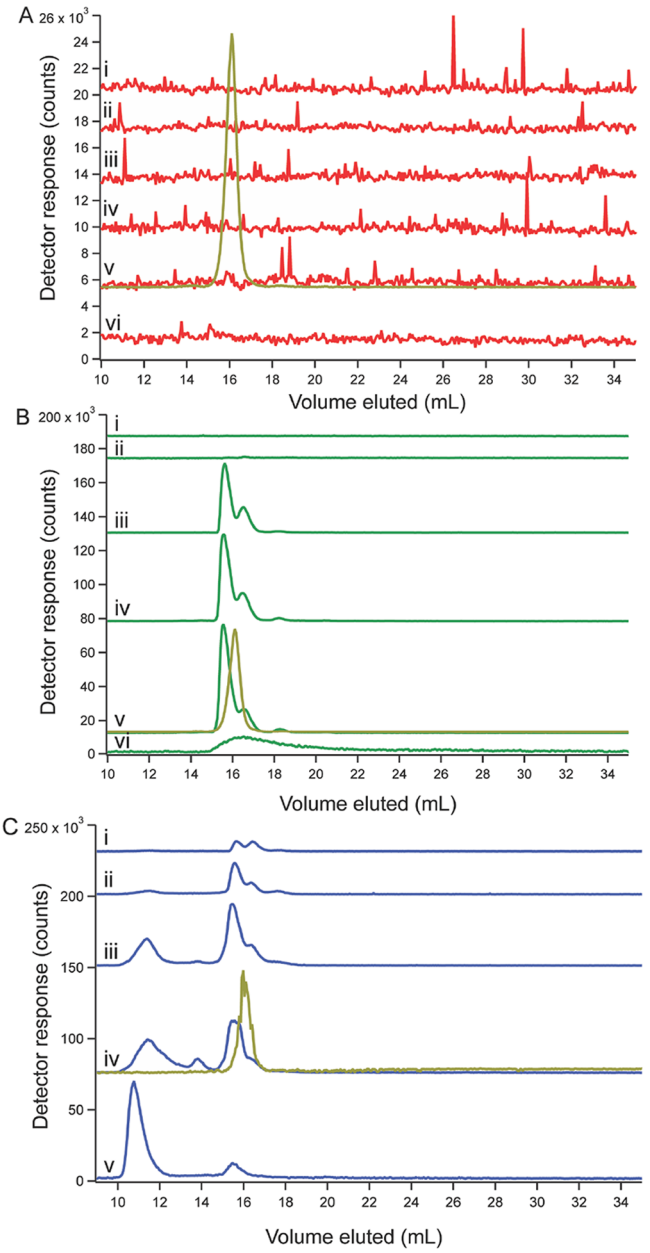

Figure 11. GSH forms complexes with Cu(II) (Panel C) and Zn(II) (Panel B) but not Fe(II) (Panel A) at pH 7.5. Panel A: (i–vi) 2 μM $FeSO_4$ plus GSH at (final mM concentration) (i) 0.5; (ii) 1; (iii) 5; (iv) 10; (v) 20; (vi) nothing added to $FeSO_4$ but mobile phase contained 1 mM GSH. Panel B: (i–vi) 2 μM $Zn(acetate)_2$ plus GSH at (final mM concentration) (i) 0.5; (ii) 1; (iii) 5; (iv) 10; (v) 20; (vi) nothing added to $Zn(acetate)_2$, but the mobile phase contained 1 mM GSH. Panel C: (i–v) 2 μM $CuSO_4$ plus GSH at (final mM concentration) (i) 0.5; (ii) 1; (iii) 5; (iv) 10 (sulfur trace was from an injection using 20 mM GSH); (v) nothing added to $CuSO_4$, but the mobile phase contained 1 mM GSH. Color coding: ^{56}Fe, red; ^{34}S, yellow; ^{66}Zn, green; ^{63}Cu, blue. Magnification factors: (Panel A) (i–vi), ^{56}Fe × 1; (v) ^{34}S × 0.1; (Panel B) (i–vi) ^{66}Zn × 1; (v) ^{34}S × 0.4; (Panel C) (i–v) ^{63}Cu × 1; (iv) ^{34}S × 0.4. A Superdex Increase column with 100 mM ABC pH 7.5 buffer was used.

With GSH included in the mobile phase, the concentration of GSH was maintained at 1 mM throughout the migration of iron down the column, approximating equilibrium conditions and giving every opportunity for an Fe(II)-GSH complex to survive column migration. No such complex was detected.

https://doi.org/10.1021/jacs.2c06625
J. Am. Chem. Soc. 2023, 145, 2104–2117

Table 1. Mössbauer Parameters for Fe(II) Standards[a]

sample	term A (larger ΔE_Q)				term B (smaller ΔE_Q)				
	δ (mm/s)	ΔE_Q (mm/s)	Γ (mm/s)	area %	δ (mm/s)	ΔE_Q (mm/s)	Γ (mm/s)	area %	APS (%)
1 mM ^{57}Fe, 2 mM ascorbate (base)	1.38	3.19	0.39	47	1.38	2.66	0.56	53	0
+ 25 mM GSH, 24 h	1.38	3.23	0.38	53	1.38	2.71	0.56	47	2.6
+ 250 mM GSH, 24 h	1.38	3.27	0.36	53	1.36	2.77	0.53	47	4.8
+ 25 mM GSH, 1 mM citrate	1.34	3.18	0.41	53	1.37	2.74	0.55	47	3.8
+ 25 mM GSH, 10 mM citrate, 24 h	1.28	3.24	0.32	47	1.31	2.85	0.46	53	8.1
+ 25 mM GSH, 1 mM ATP	1.31	3.00	0.37	84	1.37	2.44	0.53	16	14.8
+ 25 mM GSH, 10 mM ATP, 24 h	1.32	2.95	0.45	90	1.51	2.75	0.35	10	24.1

[a]Samples were prepared in the same manner, spectra were collected on the same instrument (5 K and 0.05 T parallel field), each collected immediately after another. Two-term simulations were fitted to the data using WMOSS software. The percentage shift for a parameter relative to the base condition (1 mM ^{57}Fe, 2 mM ascorbic acid) was $100 \times |P_s - P_b|/P_b$, where P_s is the value for the sample and P_b is the corresponding value for the base. APS is the average parameter shift for the first seven listed parameters, from left to right.

We also investigated Fe-GSH complex formation using MB spectroscopy. We reduced a 1 mM ^{57}Fe(III) stock solution using 2 mM ascorbic acid (final concentrations) and buffered the solution with 100 mM ABC pH 7.5. To this base solution was added various combinations of GSH, citrate, and ATP. We collected MB spectra using the same instrument, one immediately after the other, and using the same calibration. Simulations of the resulting NHHS Fe(II) quadrupole doublets (Figure S4) uniformly used two terms. All this was done to minimize uncertainties and allow MB parameters to be compared more precisely. Best-fit simulation (red lines) were generated using parameters in Table 1. Differences in all cases were modest, rendering it difficult to conclude whether complexes did or did not form. This situation suggests that in each case, Fe(II) ions were coordinated exclusively or mainly by O donors, either from waters, hydroxides, carboxylates, etc. Parameters shifted least when 25 mM GSH was included, most when ATP was included, and intermediately when citrate was included. This occurred even though the ligand/metal molar ratio favored GSH, and citrate and ATP samples were added in addition to GSH. In another experiment ^{57}Fe(III) was reduced with dithionite and half was treated with 250 mM GSH (Figure S5). The shift in parameters was again modest. Although further studies are required, these results support the conclusion that citrate and ATP form Fe(II) complexes under physiological conditions, but GSH does not.

Nor did we observe Fe(II) or Fe(III) complexes involving GSSG, Cys, Asp, Glu, or PO_4 ligands (Figure S2A, ii–vi (pH 7.5) and Figure S3 (pH 6.5)), regardless of mobile-phase pH. An Fe-His complex was typically not observed using as high as 1 mM His (Figure 3E (pH 7.5) and Figure 4F (pH 6.5)). The reported concentration of histidine in the cytosol is 68 μM.[41] The gray lines indicate absorbance at 210 nm due to the imidazole ring. Fe-His complexes either did not form or they dissociated as they migrated down the column. In one experiment, a weak Fe-His peak was observed when dithionite was included in the mobile phase (Figure 8H). However, no comigrating peak was evident in FTS even under these reducing conditions. In summary, our results suggest that iron does not form complexes with His, GSSG, Cys, Asp, or Glu under the conditions examined, and we regard them as unlikely components of the LFeP in *E. coli*.

DISCUSSION

The objective of this study was to better characterize the labile iron pool in the cytosol of *E. coli* using a combination of advanced liquid chromatography methods (with online ICP-MS detection) and Mössbauer spectroscopy. The same objective has been pursued for a half-century with significant, albeit limited, progress. Our results are schematically summarized in Figure 12. One requirement of any such investigation is to lyse cells, but this opens up the possibility that cellular contents might be altered in the process. Labile iron complexes are certainly susceptible to lysis-dependent alterations since they have an inherent tendency to dissociate. Moreover, we demonstrated here that ISCs are easily destroyed during cell lysis, even when precautions are taken to lyse cells as gently as possible. The extent of ISC degradation was lessened but not eliminated by lysing cells anaerobically. Most ISC-iron that was released during lysis became NHHS Fe(II) and likely contributed to the LFeP.

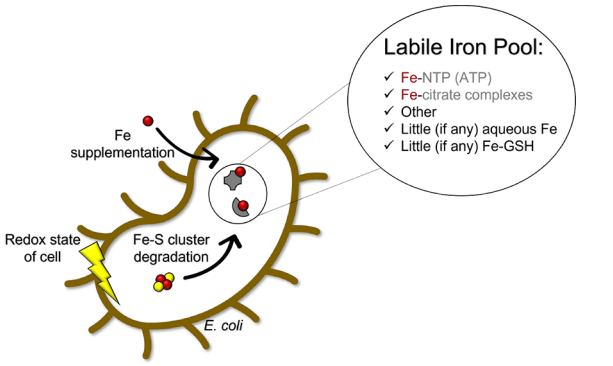

Figure 12. Summary scheme for the LFeP in *E. coli* along with factors that influence its content. Fe-citrate and Fe-NTP complexes appear to be significant components of the LFeP, whereas Fe-GSH complexes and aqueous Fe(II) do not. The level of iron supplementation in the growth medium, the extent of iron-sulfur cluster degradation during cell lysis, and the redox state of the cell can affect the composition of the LFeP.

Another challenge in characterizing the LFeP, highlighted in this study, is that the pool is probably not composed of a static group of iron complexes at a fixed concentration but rather a dynamically changing group of complexes whose concentrations vary with the degree to which the growth media is supplemented with nutrient iron. Metabolic growth mode and anaerobic/aerobic growth conditions likely also affect the composition and size of the pool.[28,30,35] In brief, the LFeP is a moving target. Future characterizations should specify the growth, harvesting, and processing conditions used.

https://doi.org/10.1021/jacs.2c06625
J. Am. Chem. Soc. 2023, 145, 2104–2117

Adding to these challenges is the diverse coordination, redox, and solubility chemistry of iron. On the other hand, iron has one advantage over other metals, namely, that it can be studied by Mössbauer spectroscopy (as long as samples can be prepared at sufficiently high concentrations). Here, we used MB spectroscopy to evaluate the redox and coordination chemistry of various iron complex standards that were considered likely candidates of the LFeP, including Fe-citrate and Fe-ATP. The MB spectra of these complexes, when reduced to the Fe(II) state, included quadrupole doublets similar to those observed in spectra of whole cells and lysates (a portion of which was the LFeP), consistent with NHHS Fe(II) coordinated by five or six O/N donor ligands.

After removing the insoluble portions of the cell lysate and passing the soluble portion through a 3 kDa cutoff membrane, we examined the FTS using size-exclusion chromatography in a refrigerated anaerobic glove box. Some batches were isolated anaerobically, and some were isolated aerobically. We prepared a variety of iron complex standards and compared their chromatographic properties to those of the LMM iron complexes detected in the FTS.

In our two previous investigations of the LFeP in *E. coli*, we detected two[30] and two to five[35] LMM Fe species. We also found that the size of the pool was affected by the concentration of iron that supplemented the growth media (80 μM Fe in the LFeP when cells were supplemented with 10 μM Fe in the growth medium and 200 μM Fe when supplemented with 100 μM Fe in the medium).[35] We were also only able to detect an Fe(*II*)-GSH complex using concentrations of GSH (50−100 mM)[35] exceeding physiological conditions.[41] Use of the chelator EDTA during cell lysis in our first study,[30] as noted,[35] may have perturbed the LFeP.

In our current study, approximately a half-dozen Fe-detected chromatography peaks were observed in FTS. Two classes of iron complexes appeared to be major components of the *E. coli* FTSs under the conditions investigated. One class involved citrate, and the other involved nucleotide triphosphates. These conclusions were based primarily on the comigration of prepared standard complexes with particular peaks in FTS traces. There were significant batch-to-batch variations. FTS appeared to contain at least two forms of Fe-citrate, perhaps more. Iron binds to the triphosphate groups of NTPs, less tightly to diphosphate groups, and not to mono-phosphate groups, confirming earlier studies.[8,46] NTPs in FTSs hydrolyze on the timescale of tens of hours, and ligand rearrangements are rapid. These factors were likely responsible for batch-to-batch variability. Further studies are required to identify the other members of the LFeP.

Aqueous iron is not a major component of the LFeP. When aqueous Fe(II) or Fe(III) complexes were added to FTS, those ions quickly coordinated available ligands in the FTS, suggesting a similar fate for any aqueous iron species that would enter the cytosol of *E. coli*, including iron from degraded ISCs. The complexes formed involved ligands of intermediate binding strength, i.e., sufficiently stable to migrate down the column but are not so stable as to be unaffected by chelators.[35]

The most surprising result of this study was that the Fe(II)-GSH complex was not a major component of the LFeP. This was unexpected since this complex is widely regarded as the dominant component of the LFeP in biological systems. We conducted many experiments to detect an Fe-GSH complex but were unable. Solutions of aqueous iron (either Fe(II) or Fe(III)) were mixed with GSH at various concentrations and at pHs ranging from 5.5 to 7.5. We injected these solutions onto the column and used the ICP-MS in efforts to observe an Fe-detected peak that either comigrated with the S-detected peak due to free GSH or at least migrated in the vicinity of the GSH peak. No such Fe-detected peak was observed. As a positive control, we prepared solutions of Zn-GSH and Cu-GSH on the same day and using the same solutions; both eluted as sharp peaks that were readily detected.

We also considered that Fe(II)-GSH might be thermodynamically stable (high k_{on}/k_{off} ratio) but kinetically unstable (i.e., rapid k_{on} and k_{off}); this could explain why the complex does not survive migration down the column but might still be present in whole intact cells. However, if this were the case, our experiments in which 1 mM GSH was used in the mobile phase should have resulted in an Fe-detected peak comigrating (or nearly comigrating) with free GSH; again, no such peak was observed. We investigated this issue using MB spectroscopy but were unable to unambiguously detect an Fe(II)-GSH complex. As a positive control, we added ATP or citrate to the solution containing Fe(II) and GSH and, in both cases, obtained some MB evidence for Fe(II)-ATP and Fe(II)-citrate complex formation.

We are currently unable to reconcile these results with previous studies showing Fe(II)-GSH complex formation. Using an experimentally determined binding constant for the Fe(II)-GSH complex, Hider and Kong simulated the distribution plot (Figure 5 of ref 32), which predicts that at pH 6.5, ∼58% of the iron should be Fe(II)-GSH, ∼35% should be aqueous Fe(II), and ∼7% should be Fe(II)-citrate (our estimates from their plot). These simulations assumed 1 μM iron, 100 μM citrate, and 2 mM GSH final concentrations. Hider and Kong concluded that Fe(II)-GSH "dominates the speciation of cytosolic Fe(II) over the Fe(II) concentration range of 10^{-7} to 10^{-5} M."[32] One possible reason for the different outcomes may be that the concentration of citrate in *E. coli* is 20-fold higher (2 mM)[37] than was assumed in their calculations and that Fe-ATP (9.6 mM in *E. coli*)[41] was not included as a competing ligand.

We also caution that the LFeP in *E. coli* and other bacteria might differ from those in eukaryotes due to differences in ligands and/or Fe concentrations. Mammals contain PCBP1/2 chaperone proteins, whereas bacteria (and yeast) do not. Philpott and coworkers found that PCBP1 coordinates Fe(II) and GSH.[47,48] When bound with protein BolA2, the resulting complex serves as a chaperone that links the LFeP to cytosolic ISC assembly. Further studies are required to understand the differences in the composition of the LFeP in bacteria vs mammalian cells.

Mössbauer Spectra. Hamed et al. reported that Fe(III) is reduced to Fe(II) in the presence of GSH,[49−51] and we confirmed that here using MB spectroscopy. They also reported that the MB spectrum of natural abundance Fe mixed with 3 equivalents of GSH prepared anaerobically at pH 7.0 exhibited a quadrupole doublet with parameters typical of NHHS Fe(II) with predominantly O/N ligands; δ = 1.32 mm/s, ΔE_Q = 3.00 mm/s.[50] Those parameters are similar to (though not exactly the same as) the MB parameters that we obtained. However, at pH 8.2, they observed an Fe(II) doublet that was fitted to two doublets - one assigned to Fe(II)-GSH (δ = 0.69 mm/s, ΔE_Q = 3.35 mm/s) and the other assigned to a green precipitated Fe(II) hydrolysis product.[51] The first doublet was only obtained when isotopically enriched ^{57}Fe was used along with 10 equivalents of GSH at pH 9. It seems

https://doi.org/10.1021/jacs.2c06625
J. Am. Chem. Soc. 2023, 145, 2104−2117

unlikely that the pH difference could explain the majorly different parameters that we obtained. Reduced rubredoxin contains a high-spin Fe(II) ion coordinated by four cysteinate ligands and exhibits a doublet with similar parameters, namely, δ = 0.65 mm/s and ΔE_Q = 3.16 mm/s.[52] Hamed et al. concluded that the Fe(II)-GSH complex is bound similarly, with deprotonated sulfur bound to Fe in addition to peptide N and carboxylate groups. In contrast, none of the doublets that we observed, from samples that contained GSH, was rubredoxin-like.

Oxidation State of Iron in the LFeP. Most iron in the cytosolic LFeP of *E. coli* is undoubtedly Fe(II), as evidenced by our MB spectra of whole cells as well as many other previous studies. However, our results also show that both oxidized and reduced iron (Fe(III) and Fe(II)) can coordinate likely ligands of the LFeP (citrate and ATP), i.e., the LFeP is not "locked in" to the Fe(II) state. For example, under conditions of oxidative stress (low reductant concentrations and/or excess O_2 or reactive oxygen species), some iron in the LFeP might be Fe(III). Numerous ligands in the cytosol, including but not limited to NTPs and citrate, are able to bind Fe(III) to yield stable, highly soluble complexes. Unlike aqueous Fe(II) or labile Fe(II) complexes, Fe(III) complexes probably do not participate in Fenton chemistry, which would offer advantages to the cell.

Comparison to Previous Studies of the LFeP. We previously reported that *E. coli* cells, grown aerobically in medium supplemented with 10 μM natural abundance Fe(III)-citrate, contained 1000 ± 300 μM Fe and that isolated cytosol contained 400 ± 200 μM Fe, and the cytosolic FTS contained 80 ± 20 μM Fe.[35] This corresponds to ∼8% of the Fe in the cell and 20% of the Fe in the cytosol due to the LFeP. Chromatograms from our previous study also revealed two to five partially resolved peaks. For cells grown on medium supplemented with 100 μM natural abundance Fe(III)-citrate, the FTS contains ∼200 μM Fe.[35] Wofford et al. reported a similar concentration for the LMM iron species in whole cells but with a wider range.[30] Overall, our estimates for the size of the LFeP in *E. coli* are higher than generally reported using chelator probes. Further studies are required to understand these differences, but our estimates of the LFeP concentration in the cell might have overestimated the endogenous LFeP concentration due to the degradation of ISCs during cell lysis and the addition of the freed iron to the labile iron pool.

CONCLUSIONS

The LFeP of isolated *E. coli* cytosol has been investigated using SEC-ICP-MS in conjunction with Mössbauer spectroscopy. We conclude that the LFeP likely...

- includes Fe coordinated to nucleotide triphosphates and Fe coordinated to citrate in various forms.
- does not include Fe-glutathione as a major component.
- does not include aqueous iron as a major component.
- includes iron from ISC degradation occurring during cell lysis.
- has a dynamic composition and concentration depending on how the cells are grown and the level of iron supplementation in the growth medium. When cells are supplemented with nutrient iron, the LFeP contains a half-dozen members.
- is not "locked in" the Fe(II) state. Under healthy metabolically active conditions, the Fe(II) state undoubtedly dominates. GSH likely functions as a reductant, in combination with NAD(*P*)H and ferric reductases,[53] to maintain the Fe(II) state of the pool. Under oxidatively stressed conditions, the possibility that the LFeP includes stable, soluble, and benign Fe(III) complexes should be considered.

ASSOCIATED CONTENT

Supporting Information

The Supporting Information is available free of charge at https://pubs.acs.org/doi/10.1021/jacs.2c06625.

(Table S1) Mössbauer simulation parameters; (Table S2) fitting parameters for chromatography simulations; (Table S3) iron concentrations for *E. coli* whole-cell lysates and cytosolic FTS; (Figure S1) SEC-ICP-MS chromatograms of aFTS at pH 5.5; (Figure S2) SEC-ICP-MS chromatograms of Fe(II) and Fe(III) weak binding ligands at pH 7.5; (Figure S3) SEC-ICP-MS chromatograms of Fe(II) and Fe(III) weak-binding ligands at pH 6.5; (Figure S4) Mössbauer spectra of Fe(II) added to 25 mM GSH, citrate and ATP; (Figure S5) Mössbauer spectra of Fe(II) added to 250 mM GSH (PDF)

AUTHOR INFORMATION

Corresponding Author

Paul A. Lindahl − *Department of Chemistry, Texas A&M University, College Station, Texas 77843-3255, United States; Department of Biochemistry and Biophysics, Texas A&M University, College Station, Texas 77843, United States;* orcid.org/0000-0001-8307-9647; Phone: 979-845-0956; Email: Lindahl@chem.tamu.edu; Fax: 979-845-4719

Authors

Hayley N. Brawley − *Department of Chemistry, Texas A&M University, College Station, Texas 77843-3255, United States*

Alexia C. Kreinbrink − *Department of Biochemistry and Biophysics, Texas A&M University, College Station, Texas 77843, United States*

Justin D. Hierholzer − *Department of Biochemistry and Biophysics, Texas A&M University, College Station, Texas 77843, United States;* orcid.org/0000-0002-0997-3971

Shaik Waseem Vali − *Department of Biochemistry and Biophysics, Texas A&M University, College Station, Texas 77843, United States*

Complete contact information is available at: https://pubs.acs.org/10.1021/jacs.2c06625

Author Contributions

[§]H.N.B. and A.C.K. contributed equally to this work.

Funding

This work was funded by the National Institutes of Health (GM127021), the National Science Foundation (MCB-1817389), and the Robert A. Welch Foundation (A1170). The content of this article is solely the responsibility of the authors and does not necessarily represent the official views of the NIH, NSF, or the Welch Foundation.

Notes

The authors declare no competing financial interest.

■ ABBREVIATIONS

AA	ammonium acetate
ABC	ammonium bicarbonate
aFTS	aerobically isolated FTS
FTS	flow-through-solution
GSH	reduced glutathione
GSSG	oxidized glutathione
HPW	high-purity water
ICP-MS	inductively coupled plasma mass spectrometry
ISC	iron−sulfur cluster
LMM	low-molecular-mass
LFeP	labile iron pool
MB	Mössbauer
NHHS	non-heme high-spin
pFTS	pseudo flow-through-solution
SEC	size-exclusion chromatography
TMG	trace-metal-grade

■ REFERENCES

(1) Chandrangsu, P.; Rensing, C.; Helmann, J. D. Metal homeostasis and resistance in bacteria. *Nat. Rev. Microbiol.* **2017**, *15*, 338−350.
(2) Mettert, E. L.; Kiley, P. J. How is Fe-S Cluster formation regulated? *Annu. Rev. Microbiol.* **2015**, *69*, 505−526.
(3) Crack, J. C.; Le Brun, N. E. Biological iron-sulfur clusters: Mechanistic insights from mass spectrometry. *Coord. Chem. Rev.* **2021**, *448*, 214171.
(4) Fontecave, M.; de Choudens, S. O.; Py, B.; Barras, F. Mechanisms of iron-sulfur cluster assembly: the SUF machinery. *J. Biol. Inorg. Chem.* **2005**, *10*, 713−721.
(5) Lindahl, P. A.; Moore, M. J. Labile Low-Molecular-Mass metal complexes in mitochondria: trials and tribulations of a burgeoning field. *Biochemistry* **2016**, *55*, 4140−4153.
(6) Jomova, K.; Valko, M. Advances in metal-induced oxidative stress and human disease. *Toxicology* **2011**, *283*, 65−87.
(7) Konopka, K.; Szotor, M. Determination of iron in acid-soluble fraction of human erythrocytes. *Acta Haematol.* **2004**, *47*, 157−163.
(8) Goucher, C. R.; Taylor, J. F. Compounds of ferric iron with adenosine triphosphate and other nucleoside phosphates. *J. Biol. Chem.* **1964**, *239*, 2251−2255.
(9) Bartlett, G. R. Iron nucleotides in human and rat red cells. *Biochem. Biophys. Res. Commun.* **1976**, *70*, 1063−1070.
(10) Bakkeren, D. L.; De Jeu-Jaspars, C. M.; van der Heul, C.; van Euk, H. G. Analysis of iron-binding components in the low molecular weight fraction of rat reticulocyte cytosol. *Int. J. Biochem.* **1985**, *17*, 925−930.
(11) Weaver, J.; Pollack, S. Low-Mr iron isolated from gunea-pig reticulocytes as AMP-Fe and ATP-Fe complexes. *Biochem. J.* **1989**, *261*, 787−792.
(12) Ma, Y.; Abbate, V.; Hider, R. C. Iron-sensitive fluorescent probes: monitoring intracellular iron pools. *Metallomics* **2015**, *7*, 212−222.
(13) Au-Yeung, H. Y.; Chan, J.; Chantarojsiri, T.; Chang, C. J. Molecular Imaging of Labile Iron(II) Pools in Living Cells with a Turn-On Fluorescent Probe. *J. Am. Chem. Soc.* **2013**, *135*, 15165−15173.
(14) Prus, E.; Fibach, E. Flow cytometry measurement of the labile iron pool in human hematopoietic cells. *Cytometry, Part A* **2008**, *73A*, 22−27.
(15) Iovan, D. A.; Jia, S.; Chang, C. J. Inorganic chemistry approaches to activity-based sensing: from metal sensors to bioorthogonal metal chemistry. *Inorg. Chem.* **2019**, *58*, 13546−13560.
(16) Rothman, R. J.; Serroni, A.; Farber, J. L. Cellular pool of transient ferric iron, chelatable by deferoxamine and distinct from ferritin, that is involved in oxidative cell injury. *Mol. Pharmocol.* **1992**, *42*, 703−710.
(17) Egyed, A.; Saltman, P. Iron is maintained as Fe(II) under aerobic conditions in erythroid cells. *Biol. Trace Elem. Res.* **1984**, *6*, 357−364.
(18) Breuer, W.; Epsztejn, S.; Cabantchik, Z. I. Iron acquired from transferrin by K562 cells is delivered into a cytoplasmic pool of chelatable iron(II). *J. Biol. Chem.* **1995**, *270*, 24209−24215.
(19) Petrat, F.; de Groot, H.; Sustmann, R.; Rauen, U. The chelatable iron pool in living cells: a methodically defined quantity. *Biol. Chem.* **2002**, *362*, 137−147.
(20) Williams, R. J. P. Free manganese(II) and iron(II) cations can act as intracellular cell controls. *FEBS Lett.* **1982**, *140*, 3−10.
(21) Thomas, F.; Serratrice, G.; Béguin, C.; Saint Aman, E.; Pierre, J. L.; Fontecave, M.; Laulhère, J. P. Calcein as a fluorescent probe for ferric iron − application to iron nutrition in plant cells. *J. Biol. Chem.* **1999**, *274*, 13375−13383.
(22) Breuer, W.; Epsztejn, S.; Cabantchik, Z. I. Dynamics of the cytosolic chelatable iron pool of K562 cells. *FEBS Lett.* **1996**, *382*, 304−308.
(23) Epsztejn, S.; Kakhlon, O.; Glickstein, H.; Breuer, W.; Cabantchik, Z. I. Fluorescence analysis of the labile iron pool of mammalian cells. *Anal. Biochem.* **1997**, *248*, 31−40.
(24) Petrat, F.; Rauen, U.; De Groot, H. Determination of the chelatable iron pool of isolated rat hepatocytes by digital fluorescence microscopy using the fluorescent probe, phen green SK. *Hepatology* **1999**, *29*, 1171−1179.
(25) Petrat, F.; de Groot, H.; Sustmann, R.; Rauen, U. The chelatable iron pool in living cells: a methodically defined quantity. *Biol. Chem.* **2002**, *383*, 489−502.
(26) Ma, Y.; de Groot, H.; Liu, Z.; Hider, R. C.; Petrat, F. Chelation and determination of labile iron in primary hepatocytes by pyridinone fluorescent probes. *Biochem. J.* **2006**, *395*, 49−55.
(27) Keyer, K.; Imlay, J. A. Superoxide accelerates DNA damage by elevating free-iron levels. *Proc. Natl. Acad. Sci. U. S. A.* **1996**, *93*, 13635−13640.
(28) Helmann, J. D. Specificity of metal sensing: iron and manganese homeostasis in Bacillus subtilis. *J. Biol. Chem.* **2014**, *289*, 28112−28120.
(29) Beauchene, N. A.; Mettert, E. L.; Moore, L. J.; Keleş, S.; Willey, E. R.; Kiley, P. J. O_2 availability impacts iron homeostasis in *Escherichia coli*. *Proc. Natl. Acad. Sci. U. S. A.* **2017**, *114*, 12261−12266.
(30) Wofford, J. D.; Bolaji, N.; Dziuba, N.; Outten, F. W.; Lindahl, P. A. Evidence that a respiratory shield in *Escherichia coli* protects a low-molecular-mass Fe^{II} pool from O_2-dependent oxidation. *J. Biol. Chem.* **2019**, *294*, 50−62.
(31) Fontenot, C. R.; Tasnim, H.; Valdes, K. A.; Popescu, C. V.; Din, H. Ferric uptake regulator (Fur) reversibly binds a [2Fe-2S] cluster to sense intracellular iron homeostasis in *Escherichia coli*. *J. Biol. Chem.* **2020**, *295*, 15454−15463.
(32) Hider, R. C.; Kong, X. L. Glutathione: a key component of the cytoplasmic labile iron pool. *BioMetals* **2011**, *24*, 1179−1187.
(33) Hider, R. C.; Kong, X. Iron speciation in the cytosol: an overview. *Dalton Trans.* **2013**, *42*, 3220−3229.
(34) Hider, R.; Aviles, M. V.; Chen, Y.-L.; Latunde-Dada, G. O. The Role of GSH in Intracellular Iron Trafficking. *Int. J. Mol. Sci.* **2021**, *22*, 1278.
(35) Brawley, H. N.; Lindahl, P. A. Low-molecular-mass labile metal pools in *Escherichia coli*: advances using chromatography and mass spectrometry. *J. Biol. Inorg. Chem.* **2021**, *26*, 479−494.
(36) Nguyen, T. Q.; Kim, J. E.; Brawley, H. N.; Lindahl, P. A. Chromatographic detection of low-molecular-mass metal complexes in the cytosol of *Saccharomyces cerevisiae*. *Metallomics* **2020**, *12*, 1094−1105.
(37) Brawley, H. N.; Lindahl, P. A. Direct detection of the labile nickel pool in *Escherichia coli*: new perspectives on labile metal pools. *J. Am. Chem. Soc.* **2021**, *143*, 18571−18580.
(38) Cahill, J.; Young, R. Phage lysis: multiple genes for multiple barriers. *Adv Virus Res* **2019**, *103*, 33−70.

https://doi.org/10.1021/jacs.2c06625
J. Am. Chem. Soc. 2023, 145, 2104−2117

(39) Lutz, R.; Bujard, H. Independent and tight regulation of transcriptional units in *Escherichia coli* via the LacR/O, the TetR/O, and AraC/I_1-I_2 regulatory elements. *Nucleic Acids Res.* **1997**, *25*, 1203−1210.
(40) Adam, F. I.; Bounds, P. L.; Kissner, R.; Koppenol, W. H. Redox properties and activity of iron-citrate complexes: evidence for redox cycling. *Chem. Res. Toxicol.* **2015**, *28*, 604−614.
(41) Bennett, B. D.; Kimball, E. H.; Gao, M.; Osterhout, R.; VanDien, S. J.; Rabinowitz, J. D. Absolute metabolite concentrations and implied enzyme active site occupancy in *Escherichia coli*. *Nat. Chem. Biol.* **2009**, *5*, 593−599.
(42) Mayhew, S. G. The redox potential of dithionite and SO2- from equilibrium reactions with flavodoxins, methyl viologen, and hydrogen plus hydrogenase. *Eur. J. Biochem.* **1978**, *85*, 535−547.
(43) Cockrell, A. L.; Holmes-Hampton, G. P.; McCormick, S. P.; Chakrabarti, M.; Lindahl, P. A. Mössbauer and EPR study of iron in vacuoles from fermenting *Saccharomyces cerevisiae*. *Biochemistry* **2011**, *50*, 10275−10283.
(44) Walsh, M. . J.; Ahner, B. A. Determination of stability constants of Cu(I), Cd(II), & Zn(II) complexes with thiols using fluorescent probes. *J. Inorg. Biochem.* **2013**, *128*, 112−123.
(45) Aliaga, M. E.; López-Alarćon, C.; Bridi, R.; Speisky, H. Redox-implications associated with the formation of complexes between copper ions and reduced or oxidized glutathione. *J. Inorg. Biochem.* **2016**, *154*, 78−88.
(46) Richter, Y.; Fischer, B. Characterization and elucidation of coordination requirements of adenine nucleotides complexes with Fe(II) ions. *Nucleosides, Nucleotides, Nucleic Acids.* **2003**, *22*, 1757−1780.
(47) Philpott, C. C.; Patel, S. J.; Protchenko, O. Management versus miscues in the cytosolic labile iron pool: the varied functions of iron chaperones. *Biochim. Biophys. Acta − Mol. Cell Res* **2020**, *1867*, 118830.
(48) Patel, S. J.; Frey, A. G.; Palenchar, D. J.; Achar, S.; Bullough, K. Z.; Vashisht, A.; Wohlschlegel, J. A.; Philpott, C. C. A PCBP1-BolA2 chaperone complex delivers iron for cytosolic [2Fe-2S] cluster assembly. *Nat. Chem. Biol.* **2019**, *15*, 872−881.
(49) Hamed, M. Y.; Silver, J.; Wilson, M. T. Studies of the reactions of ferric iron with glutathione and some related thiols. *Inorg. Chim. Acta* **1983**, *78*, 1−11.
(50) Hamed, M. Y.; Silver, J. Studies of the reactions of ferric iron with glutathione and some related thiols. Part II. Complex formation in the pH range three to seven. *Inorg. Chim. Acta* **1983**, *80*, 115−122.
(51) Hamed, M. Y.; Silver, J.; Wilson, M. T. Studies of the reactions of ferric iron with glutathione and some related thiols. Part III. A study of the iron catalyzed oxidation of glutathione by molecular oxygen. *Inorg. Chim. Acta* **1983**, *80*, 237−244.
(52) Rao, K. K.; Evans, M. C. W.; Cammack, R.; Hall, D. O.; Thompson, C. L.; Jackson, P. J.; Johnson, C. E. Mössbauer effect in Rubredoxin. Determination of the hyperfine field of the iron in a simple iron−sulphur protein. *Biochem. J.* **1972**, *129*, 1063−1070.
(53) Schröder, I.; Johnson, E.; de Vries, S. Microbial ferric ion reductases. *FEMS Microbiol. Rev.* **2003**, *27*, 427−447.

https://doi.org/10.1021/jacs.2c06625
J. Am. Chem. Soc. 2023, 145, 2104−2117